ADVANCED SUSTAINABLE SYSTEMS
www.advsustainsys.com

Sulfonated Cellulose Membranes: Physicochemical Properties and Ionic Transport versus Degree of Sulfonation

*Sanna Lander, Johan Erlandsson, Mikhail Vagin, Viktor Gueskine, Leena Korhonen, Magnus Berggren, Lars Wågberg, and Xavier Crispin**

The next generation of green ion selective membranes is foreseen to be based on cellulosic nanomaterials with controllable properties. The introduction of ionic groups into the cellulose structure via chemical modification is one strategy to obtain desired functionalities. In this work, bleached softwood fibers are oxidatively sulfonated and thereafter homogenized to liberate the cellulose nanofibrils (CNFs) from the fiber walls. The liberated CNFs are subsequently used to prepare and characterize novel cellulose membranes. It is found that the degree of sulfonation collectively affects several important properties of the membranes via the density of fixed charged groups on the surfaces of the CNFs, in particular the membrane morphology, water uptake and swelling, and correspondingly the ionic transport. Both ionic conductivity and cation transport increase with the increased level of sulfonation of the starting material. Thus, it is shown that the chemical modification of the CNFs can be used as a tool for precise and rational design of green ion selective membranes that can replace expensive conventional fluorinated ionomer membranes.

1. Introduction

Ion selective membranes constitute a key component in several technologies for large scale energy storage, such as redox flow batteries and electrolyzers. The membrane performance in those devices is characterized by properties including ionic conductivity, crossover mitigation, and long-term stability. Actually these membranes are made of synthetic polymers and dominated by Nafion, the perfluorinated sulfonic material.[1,2] The production of membranes from petrochemicals in general and polyfluorinated chemicals in particular are problematic from a sustainability perspective, and the cost of Nafion is particularly high.[3] Discovering ways to replace these materials without sacrificing the functionality of the components would constitute a big step forward on the route to green energy storage. In recent years there has emerged an interest in trying to replace traditional ion exchange membranes with membranes from bio-based and renewable materials to reduce production costs, improve functionality, and minimize environmental impact.[4–6]

Cellulosic nanomaterials can be suitable as starting material for the next-generation of ion selective membranes due to their favorable properties such as abundancy, low cost, processability, chemical and mechanical properties, nanodimension of cellulose domains, and the versatility of functionalization methods available for those cellulose domains.[7] This class of nanomaterial has already been extensively investigated in gas barrier and filtration applications.[8–10] The utilization of nanocellulose in aqueous environments requires crosslinking strategy to control swelling and to obtain wet stability. Crosslinking can be realized via additives or direct chemical modification of the material.[11–13]

Membranes produced from cellulose nanofibrils (CNFs) or nanocrystals have been employed as a medium to transport protons in devices such as hydrogen fuel cells and redox flow batteries.[14–16] The abundant hydroxyl groups on the fibril- or crystal surfaces in combination with ionic groups introduced via chemical modification give these materials a propensity for proton conduction, even at high temperatures where commercial membranes such as Nafion have suboptimal performance due to dehydration.[14]

Oxidatively sulfonated cellulose obtained via periodate oxidation followed by bisulfite sulfonation has been proposed as a promising material for production of ion selective membranes for electrochemical energy devices employing liquid electrolytes

S. Lander, M. Vagin, V. Gueskine, M. Berggren, X. Crispin
Laboratory of Organic Electronics
Department of Science and Technology
Linköping University
Norrköping SE-601 74, Sweden
E-mail: xavier.crispin@liu.se

S. Lander
BillerudKorsnäs Gruvön
Grums SE-664 33, Sweden

J. Erlandsson, L. Wågberg
Fibre and Polymer Technology
Division of Fibre Technology
KTH Royal Institute of Technology
Stockholm SE-100 44, Sweden

L. Korhonen
BillerudKorsnäs Frövi
Frövi SE-718 80, Sweden

M. Berggren, L. Wågberg, X. Crispin
Wallenberg Wood Science Centre
Fibre and polymer Technology
KTH Royal Institute of Technology
Stockholm SE-100 44, Sweden

The ORCID identification number(s) for the author(s) of this article can be found under https://doi.org/10.1002/adsu.202200275.

DOI: 10.1002/adsu.202200275

(e.g., electrolyzers and redox flow batteries). Indeed, the resulting cellulose membrane possesses a dual function: i) the cross-linkable aldehyde groups,[12,17] incorporate wet stability; and ii) the sulfonated groups improve the cationic transport. This modification route has been used to produce ionomer-like material for use in fuel cells in a humid but not liquid environment, both as freestanding and spray-deposited membranes.[18] Recently, the same strategy has been proposed for organic redox flow batteries with promising results.[19]

Ion transport through wet polymer membranes with charged pores of nanoscale diameter is complex and depends on several fundamental membrane properties such as pore size and microstructure, electrolyte uptake, degree of swelling, and fixed charge density.[20,21] Despite many years of active research, several phenomena related to ion transport in membranes remain poorly understood, especially in relation to the employment of such membranes in electrochemical applications. Now the field of cellulose membranes designed for ionic transport is new; as a consequence, little is known on the properties of functional cellulosic nanomaterials and their electrochemical behavior in liquid electrolytes.

In this work, based on the first success of using sulfonated cellulose membranes in organic redox flow batteries, we chemically control the degree of sulfonation in the cellulosic membranes and study how it affects important physicochemical and ionic transport properties of the membranes in a liquid electrolyte.

2. Experimental Section

2.1. Materials

Never dried, fully bleached and unbeaten softwood fibers were supplied by BillerudKorsnäs (Gruvön pulp mill, Grums, Sweden). Sodium metabisulfite was purchased from Alfa Aesar GmBH Co KB (Karlsruhe, Germany), sodium metaperiodate, hydroxylamine hydrochloride, sodium chloride, and potassium chloride were all purchased from VWR International (Radnor, USA). Branched polyethylene imine (PEI) with a molecular weight 60 kDa was purchased as a 50 wt% aqueous solution from Arcos Organics (USA). All chemicals were used as received.

2.2. Oxidation and Sulfonation of Cellulose

Periodate oxidation of the bleached softwood fibers was performed by adding sodium periodate to a fiber dispersion of 20 g L^{-1} in deionized water, using an earlier described procedure.[22] The reaction was performed in the absence of light to avoid photo-induced side reactions[23] under stirring for 30 min at 50 °C. Isopropanol at 6.3 wt% was used as a radical scavenger. The concentration of $NaIO_4$ was altered to tune the aldehyde content. A linear relationship between reagent concentration and degree of oxidation was assumed. To obtain samples with a different degree of sulfonation but with basically constant residual amount of aldehyde groups, the parameters that were altered were the initial degree of oxidation and the bisulfite concentration. The sulfonation step was performed by adding bisulfite to the oxidized fibers redispersed to a concentration of 20 g L^{-1}, with a reaction time of 2 h at room temperature under stirring. All reaction parameters are summarized in **Table 1**. After each reaction the pulp was thoroughly washed with deionized water. After the periodate oxidation, the pulp was kept at a relatively low solids content, to ensure that an unwanted crosslinking between aldehydes did not occur, which could potentially make the cellulose less reactive to the sulfonation. Deionized water was used through all experiments unless otherwise stated.

2.3. Aldehyde Content Determination

The content of aldehyde groups in the oxidized fibers was measured by reaction of the fibers with hydroxylamine followed by titration with sodium hydroxide to determine the amount of stoichiometrically released protons.[24] In short, 0.1 g of dry oxidized fibers was dispersed in 30 mL of hydroxylamine hydrochloride solution with the pH adjusted to 4. The dispersion was left to react for 2 h at room temperature after which the dispersions were titrated back to pH 4 using 0.1 M NaOH. The exact dry weight of the fibers in the sample was determined by filtering the fiber dispersion on a preweighed filter followed by drying overnight at 105 °C and weighing. The amount of aldehydes present in the sample was calculated from the moles of NaOH consumed in the titration and normalized by the dry sample weight. Two measurements were performed per sample (see Table S1, Supporting Information). The residual aldehyde content after the sulfonation reaction was obtained by subtracting the total charge, corresponding to sulfonated groups, from the original aldehyde content calculated as moles per gram of fibers. Since the sulfonation occurs only at the aldehyde groups, it can be assumed that the subtraction of the total charge (corresponding to the amount of sulfonated groups) from the original aldehyde content is a good estimate for the amount of residual aldehydes.

2.4. Determination of Total Charge

The total amount of sulfonic acid groups present after the sulfonation reaction was determined via conductometric titration

Table 1. Reaction conditions and resulting content of aldehyde- and sulfonate groups in the fibers after the two modification steps.

Batch	$NaIO_4$ [g/g fiber]	COH content [mmol g^{-1}]	$Na_2S_2O_5$ [g/g fiber]	Total charge [mmol g^{-1}]	Residual aldehyde content [mmol g^{-1}]
SDAC1	1.0	1.0	0.5	0.34	0.7
SDAC2	2.0	1.6	1.5	0.74	0.9
SDAC3	2.5	1.7	2.0	1.05	0.7
SDAC4	3.0	2.1	2.5	1.39	0.7

of the modified fibers. The amount of weak acid groups in the starting material was assumed to be negligible.[25] A Metrohm Conductometric Titrator (Herisau, Switzerland) was used to perform the conductometric titrations. Prior to titrating the fibers were converted to proton form by ion exchange in HCl solution at pH 1 for 30 min, and thereafter washed with deionized water until reaching a conductivity of <5 μS cm^{-1}. Approximately 0.2 g of dry fibers was dispersed in 500 mL water containing 10 mL of 0.1 M NaCl. The dispersion was subsequently bubbled with N_2-gas for 15 min to expel any dissolved CO_2 and then titrated with 0.1 M NaOH. The conductivity of the dispersion was continuously monitored during the titration. The amount of sulfonic acid groups present in the fibers were calculated from the number of moles of NaOH needed to reach the bottom of the V-shaped curve. This number was normalized by the exact dry weight of the sample obtained after drying at 105 °C overnight and weighing. Two measurements were performed per sample (see Table S2, Supporting Information).

2.5. Attenuated Total Reflectance-Fourier-Transform Infrared Spectroscopy (ATR-FTIR)

To further establish the chemical modification of the cellulose, FTIR spectra were collected in the ATR mode for each batch of sulfonated fibers using a Bruker Alpha instrument. The measurements were performed for fiber sheets with a grammage of 30 g m^{-2} prepared by vacuum filtration. Additionally, a spectrum was obtained from the unmodified pulp as a reference.

2.6. Homogenization and Film Preparation

A microfluidizer M110EH Microfluidics (MA, USA) was used to homogenize the oxidatively sulfonated fibers, thereby releasing the elementary fibrils from the fiber wall. The fibers were passed two times through two chambers of 200 and 100 μm channel width, respectively, in series. The pressure was kept at 1500 bar during all passes.

To prepare films from the obtained sulfonated CNFs, vacuum filtration was used for dewatering. Durapore DVPP membranes from Merck Millipore with a pore size of 0.65 μm were used as a substrate for the filtration. Fibril suspensions were prepared at a concentration of 0.1 wt% in deionized water and were stirred overnight with magnetic stirrer prior to film fabrication. After the dewatering step, the films were dried using the drying station of a Rapid Köthen sheet former (PTI, Pettenbach, Austria), at 93 °C for 10 min. The resulting films were freestanding, transparent, and could easily be peeled off of the Durapore-filters.

2.7. Atomic Force Microscopy (AFM) and Zeta Potential of Fibrils

AFM imaging was used to examine the sulfonated CNFs adsorbed onto freshly cleaved and PEI-coated mica surfaces. In these measurements the PEI was first adsorbed by submersion of the mica surface in a 0.1 g L^{-1} PEI solution for 30 s followed by excessive rinsing with Milli-Q water. The CNFs were subsequently adsorbed by submersion of the PEI-treated mica in a 0.1 g L^{-1} CNF dispersion for 30 s followed by rinsing and drying in a flow of N_2 gas. The adsorbed CNFs were finally imaged in air using a Bruker Multimode 8 (Bruker, Santa Barbera, CA) AFM running in the ScanAsyst mode with a cantilever having a nominal tip radius of 2 nm (SCANASYST-AIR, Bruker, Camarillo, CA).

The zeta potential of the sulfonated CNFs was measured using a Malvern Zetasizer PRO (Malvern Panalytical, Malvern, UK). Fibril suspensions were prepared at a concentration of 0.1 wt% and adjusted to pH 4. NaCl was then added to a concentration of 5 mM.

2.8. Surface Morphology and Porosity of Membranes

To study the surface morphology of the sulfonated cellulose membranes, a Jeol JSM-7900F low vacuum scanning electron microscope (SEM) equipped with an Oxford Instruments X-Max EDS detector was used. Surface scans were obtained on both sides of the membranes, at magnifications ranging from 1000× to 50 000×. For the surface scans at high magnifications the membranes were lightly coated with Au by sputtering for 10 s. Cross-sections were prepared by freezing the membranes in liquid nitrogen and thereafter breaking them. The cross-sections were scanned in their uncoated state under low-vacuum in nitrogen gas atmosphere. Additionally, energy dispersive spectroscopy was used to study the elemental composition of the two sides of the membranes respectively. These measurements were also performed for uncoated membranes under low vacuum in nitrogen gas atmosphere.

Porometry measurements were performed using a liquid–liquid porometer (POROLIQ1000ML, POROMETER, Belgium) using water–isobutanol combination with an exceptionally low interfacial tension of 2 mN m^{-1}.

2.9. Small Angle X-Ray Scattering (SAXS)

The sulfonated cellulose membranes were also characterized using SAXS in dry and water swollen state. An Anton Paar SAXSpoint 2.0 instrument equipped with a Microsource X-ray source (Cu Kα radiation, wavelength 0.15 418 nm) and a Dectris 2D CMOS Eiger R 1M detector with a 75 × 75 μm^2 pixel size was used for the measurements. The membranes were soaked in deionized water for 24 h prior to the measurements in water swollen state. Samples of appropriate size were prepared and placed in the sample holder.

2.10. Water Uptake

The water uptake of the membranes was measured gravimetrically. The membranes were immersed fully in deionized water for >1 h after which excess water on the membrane surface was removed using blotting paper lightly without applying

pressure followed by weighing to obtain the wet membrane weight (W_{wet}). The dry membrane weight (W_{dry}) was obtained by weighing after drying the membrane at 80 °C overnight. The water uptake (W.U.) of the membranes was then obtained according to the equation

$$\text{W.U.}(\%) = \frac{W_{wet} - W_{dry}}{W_{dry}} \times 100 \quad (1)$$

2.11. Ion Exchange Capacity

The ion exchange capacity of the membranes was obtained via titration. The membranes were first converted to proton form by immersion in HCl solution at pH 1 for 30 min, followed by thorough rinsing in deionized water to remove excess acid as well as light blotting of the membrane surface to remove excess liquid. The membranes were thereafter immersed in a 2 M NaCl solution of known pH and left overnight to ion exchange. Finally, the membranes were removed from the solution and their exact dry weights determined as previously described. The solution was titrated back to the starting pH using 0.001 M NaOH. The ion exchange capacity (IEC) was calculated according to the equation

$$\text{IEC} = \frac{C_{NaOH} V_{NaOH}}{W_{dry}} \quad (2)$$

2.12. Membrane Resistance Measurements

The resistance of the membranes was determined using a symmetric H-cell (Scribner Associates Inc., Southern Pines, USA) specialized for membrane characterization. A four-electrode setup was used, consisting of two platinum mesh electrodes and two Ag/AgCl reference electrodes, the latter situated at the end of Luggin capillary probes with openings positioned at a fixed distance from the membrane. The resistance was determined from the slope of the linear sweep curve, plotted as $V(I)$ for each membrane, according to Ohm's law. The cell resistance without membrane was obtained and subtracted from the measured cell resistance for each membrane to obtain the resistance contribution of the membranes. Stacks of 1–3 membranes were measured for each level of sulfonation.

Additionally, electrochemical impedance spectroscopy was used to measure the membrane resistance at different electrolyte concentrations. For this purpose, membranes presoaked in electrolyte solution of the relevant concentration were stacked between two titanium plate electrodes. The membrane resistances were obtained as the high-frequency intercepts of the real axis in the Nyquist plots.

2.13. Membrane Potentials and Transport Numbers

The apparent transport numbers of co- and counter ions in the sulfonated cellulose membranes were determined by measuring the membrane potential according to the well-known electromotive force method, in which the transport numbers are obtained according to the equation

$$E = (t_+ - t_-)\frac{RT}{F}\ln\frac{C_{high}}{C_{low}} \quad (3)$$

where E is the membrane potential, t_+ and t_- are the apparent transport numbers of the cations and anions, respectively, R is the universal gas constant, T is the temperature in Kelvin, F is Faraday's constant, and C_{high} and C_{low} denote the concentrations of electrolyte on the two sides of the membrane. The transport numbers obey the condition $t_+ + t_- = 1$.

The measurements of membrane potentials were performed using the membrane H-cell with two Ag/AgCl reference electrodes situated in the Luggin capillary probes. The concentration ratio of the KCl electrolyte in the two compartments was 2:1.

3. Results and Discussion

3.1. Oxidation and Sulfonation of Cellulose

To study the effect of increasing the degree of sulfonation of the starting material on the membrane properties, four batches of oxidatively sulfonated fibers were produced from the bleached unbeaten softwood fibers by the two-step oxidative sulfonation route. Using the sequential periodate oxidation and bisulfite sulfonation (**Figure 1**) fibers with a constant aldehyde content and four different levels of sulfonation were prepared. The samples are called SDAC1–SDAC4, from Sulfonated DiAldehyde Cellulose. Table 1 summarizes all the reaction conditions and the final composition of the prepared fibers. Figure 1 illustrates the dual functionality obtained via the oxidative sulfonation of cellulose, with ionic sulfonates and crosslinkable aldehydes by formation of hemiacetals.

The amounts of reagents used in the oxidation and sulfonation steps respectively are given in Table 1, along with the carbonyl contents after the oxidation step, the total charge as measured by conductometric titration after the sulfonation step and the carbonyl content measured after the sulfonation step, corresponding to the residual crosslinkable aldehyde groups in the final material.

ATR-FTIR spectra were obtained from the sulfonated fibers as a complement to the total charge measurements to further characterize the chemical modification. The ATR-FTIR spectra of SDAC1–SDAC4 as well as a reference sample of the unmodified softwood fibers are shown in Figure S1 of the Supporting Information. By subtracting the reference to obtain a difference spectrum for each sample the changes in absorbance upon oxidative sulfonation become evident, as shown in **Figure 2**. Novel peaks associated with SO_2 vibrations indicative of sulfonation appear at 628 and 1145 cm^{-1},[26] and in the region around 1180–1220 cm^{-1} which can be assigned to the S=O stretching.[27] A minor peak is also observed at 882 cm^{-1}, which is most likely due to the formation of hemiacetals via aldehyde groups.[17]

3.2. AFM and Zeta Potential of Fibrils

Atomic force microscopy height images of SDAC CNFs adsorbed onto mica are shown in **Figure 3**. In the AFM height

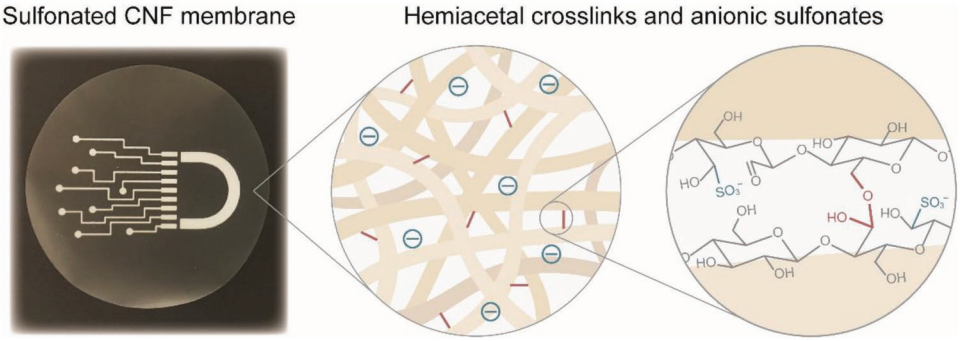

Figure 1. Schematic, depicting the two-step chemical modification of periodate oxidation followed by sulfonation of the cellulose (top). Photograph of sulfonated cellulose membrane, and illustration showing the crosslinking mechanism of aldehyde groups forming hemiacetals (bottom).[19]

images, the CNFs obtained from the sulfonated and homogenized fibers are clearly visible and all the observed CNFs have nanoscale dimensions similar to those of, e.g., TEMPO-oxidized CNFs[28] and carboxymethylated CNFs.[29] This indicates that the sequential periodate oxidation and sulfonation reactions are only occurring on the surfaces of the CNFs within the fiber wall and that the modified CNFs are individually liberated by the high-pressure homogenization. The CNFs of all four SDAC batches have similar magnitudes of the height/width dimension (≈3 nm) as determined by height profiles obtained with AFM, whereas the average length of the fibrils appear to decrease with increasing sulfonation (from ≈600 to ≈300 nm; **Table 2**). This indicates that the more the fibrils are charged, the more prone they are to breaking during the high-pressure homogenization procedure. It is also observed that a seemingly larger quantity of fibrils is adsorbed onto the mica substrates for the more highly charged fibrils.

The zeta potentials of the fibrils measured at pH 4 (Table 2) showed a trend of increasingly negative values as expected because of the increase amount of negatively charged sulfonate groups. The zeta potentials are lower than what is usually found for fibrils of similar charge densities due to carboxylate groups,[26] but correspond well to previously reported values for sulfonated CNFs.[28]

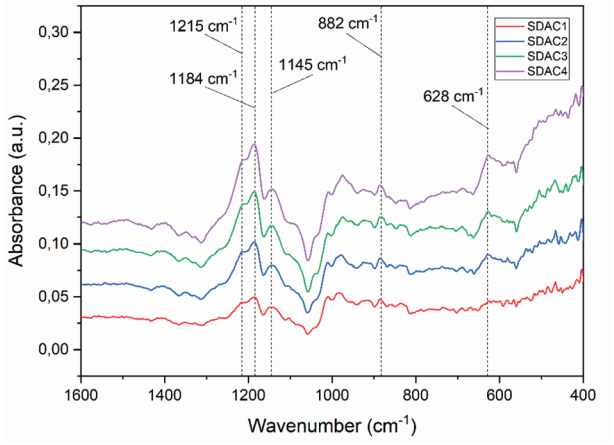

Figure 2. ATR-FTIR spectra of SDAC1–4 with the spectrum of the reference material subtracted to elucidate changes in absorbance.

3.3. Membrane Preparation and Physicochemical Properties

Membranes were successfully prepared by the dewatering and constrained drying of the SDAC CNFs using vacuum filtration of the prepared colloidal dispersions and the Rapid Köthen drying unit. The time needed to dewater the dispersions increased linearly, from 1 to 5.5 h for films of ≈30 g m^{-2} (**Table 3**), with increased degree of sulfonation, which is expected since sulfonate groups has the capability to retain water.[30] The membrane thickness could be controlled via the density of fibrils used, for 30 g m^{-2} the usual thickness was 20–25 µm.

The ion exchange capacity of the formed membranes increased for high sulfonation degree and was found to be between 14% and 29% of the corresponding total charge density measured on the fibers prior to homogenization (**Figure 4**). This indicates that charged entities are lost in one of the processing steps, most likely during the vacuum filtration where highly charged polymer chains on the fibril surfaces may have dissolved and been able to escape through the pores of the Durapore filter membranes. To test if charged material is lost during the vacuum filtration process, membranes were produced as described before and the filtrate was collected and titrated to determine its total charge content via particle charge titration (Stabino, Omega Scientific). Charged material was detected in all four samples, indeed supporting that some fibril fragments pass through the filters during the vacuum filtration for these modified materials.

The water uptake of the membranes increased linearly with degree of sulfonation (Figure 4), to a maximum of ≈180% for SDAC4; which is representing the increase in osmotic pressure with the increasing charge. However, the water uptake is not directly proportional to the ion exchange capacity since there exists a background water uptake in the cellulose fibril network due to nonionic contributions from cellulose–water interactions and network deformation.[31]

Elemental analysis by energy dispersive spectroscopy on the surfaces of the films indicate sulfur contents of on average 0.17%, 0.52%, 0.85%, and 1.24%, respectively for SDAC1–4 (Table S4, Supporting Information), showing that the increase in sulfonation as determined by the conductometric titration and ATR-FTIR also translates to the membranes. Calculating membrane sulfur content in weight percent from

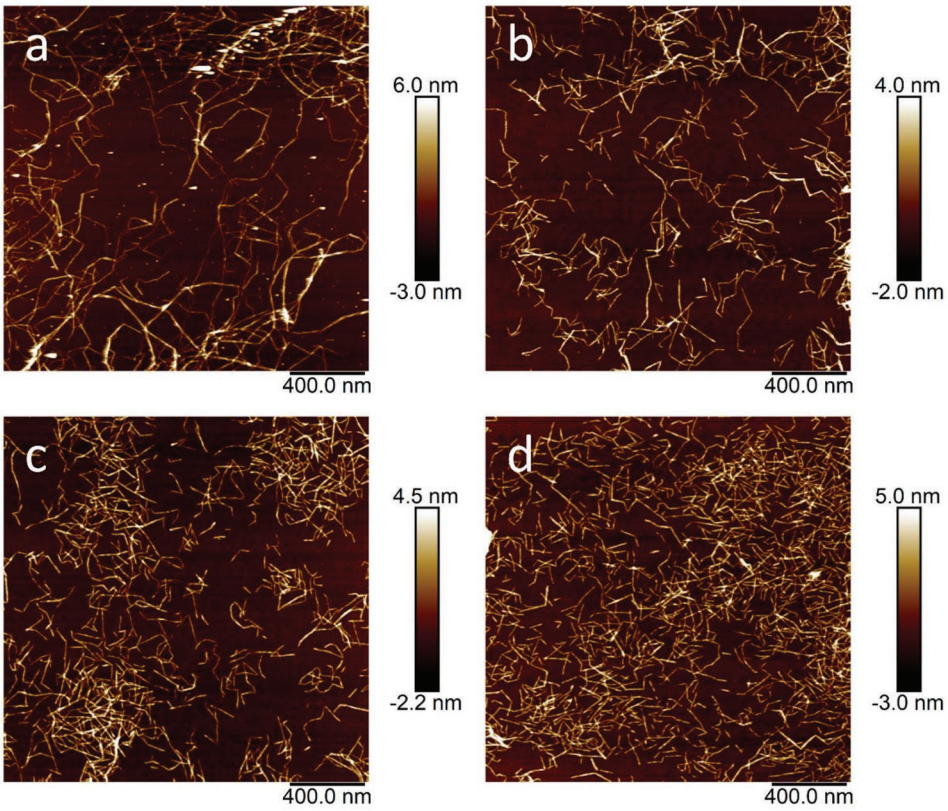

Figure 3. AFM images showing the fibrils from the batches SDAC1-4, a) SDAC1, b) SDAC2, c) SDAC3, and d) SDAC4.

the ion exchange capacity data gives corresponding values of 0.15%, 0.56%, 0.82%, and 1.30%, respectively, showing good agreement between the methods and further supporting the hypothesis that charged material is lost during the membrane fabrication process.

3.4. Porosity and Surface Structure

SAXS was used to assess changes in the structure of the sulfonated cellulose membranes upon swelling in water. For this purpose, membranes from the batches of lowest and highest degree of sulfonation (SDAC1 and SDAC4) were studied. The SAXS spectra obtained from membranes in dry and wet state respectively showed a larger relative increase in intensity for SDAC4 compared to SDAC1 in the wet state (**Figure 5**), indicating a stronger effect on the microstructure due to swelling.

Table 2. Characteristics of sulfonated CNFs. The zeta-potential was determined in 5 mM NaCl supporting electrolyte.

Batch	Fibril height/width [nm]	Fibril length [nm]	Zeta potential (pH 4) [mV]
SDAC1	3.4	635	−14.5 ± 1.9
SDAC2	3.2	402	−18.4 ± 3.0
SDAC3	3.0	318	−22.8 ± 1.0
SDAC4	3.5	317	−26.3 ± 0.7

To fit the SAXS data obtained from the membranes in the wet state, a two-stage model was used[15]

$$I(q) = \frac{a}{q^n} + b\exp\left(-\frac{(q * r_g)^2}{3}\right) + c \quad (4)$$

The first term in Equation (1) is a power law containing the Porod exponent, n, which relates to the complexity of the network. The second term is a Gaussian containing a radius of gyration, r_g, which in our system correspond to the void size, i.e., the pore size in the membranes. The factors a and b are scaling factors and c is a constant background term.

From the fitting parameters (Table S3, Supporting Information), it was possible to extract approximate pore sizes of 3.0 and 3.2 nm for SDAC1 and SDAC4, respectively, in the water-swollen state, indicating a slightly larger pore size due to higher swelling for the membrane with a higher density of sulfonated groups which is in agreement with the results from water uptake measurements. The Porod exponent was found to be 1.9 for SDAC1 and 1.5 for SDAC4, respectively. This relates to the complexity and structure of the network, where $1 < n < 2$ describes a branched structure with a 1D backbone. The lower exponent obtained for SDAC4 can be interpreted as a more dissociated fibril network due to increased swelling.[11,32]

Liquid–liquid porometry of the membranes revealed no evident difference in the through-pore size related to sulfonation degree. The mean pore size was close to 2.5 nm for all

Table 3. Physicochemical properties of sulfonated cellulose membranes SDAC1–4.

Membrane	Approximate dewatering time [h]	Water uptake [%]	Ion exchange capacity [μeq. g^{-1}]	S content EDS [%]	S content calc. from IEC [%]
SDAC1	1.0	97	46	0.17	0.15
SDAC2	2.5	142	176	0.52	0.56
SDAC3	4.0	162	257	0.85	0.82
SDAC4	5.5	182	404	1.24	1.30

membranes measured. A representative porometry curve is shown in Figure S1 of the Supporting Information. It should be noted that the liquid–liquid porometry method is only capable of measuring the interconnected pores through the samples and not so-called closed or blind pores.

The comparison of the results obtained from liquid–liquid porometry and SAXS for SDAC1 and SDAC4 (**Table 4**) reveals a slightly larger increase in pore size upon swelling with water for SDAC4 (2.5 to 3.2 nm) than for SDAC1 (2.5 to 3.0 nm). This is in line with the higher water uptake observed for SDAC4 and is a consequence of the higher density of sulfonate groups in SDAC4. Importantly, those results demonstrate that the present fabrication technique creates membranes with nm sized pores both in the wet and dry state.

Imaging of the surfaces of the uncoated membranes by environmental SEM showed an asymmetry between the top and bottom side, where the bottom side has micrometer-sized irregularities most likely originating from the contact with the Durapore-membrane in the vacuum filtration process (Figures S2–S5, Supporting Information). For SDAC4 the irregularities were also visible on the top side of the membrane. On a smaller scale, the membranes were observed to have a nanoporous surface structure, the apparent pore sizes decreasing with increased sulfonation (**Figure 6**). This nanoporous structure was similar on the top and bottom sides of the membranes. For the CNFs with a high degree of modification there is a large amount of small fibril fragments present that contribute to the dense surface pore structure.

Membrane cross-sections prepared by breaking them after freezing in liquid nitrogen are compared at the same magnification of 3000× in **Figure 7**. A trend is observed where the compactness and homogeneity of the membrane cross-sections are enhanced for high sulfonation degree. Note that a similar trend was observed on the surface morphology of the membrane. In SDAC1 a lamellar sheet structure is observed, including some irregularities and these phenomena occur to a lesser degree in SDAC2 and SDAC3, while SDAC4 presents an almost perfectly smooth cross-section. As mentioned above, this is likely due to the ability of the highly surface modified short fibrils to pack closely into dense homogeneous layers instead of interacting to form fibril bundles during the film formation process. The lamellar structures of these types of nanopapers have been detected before and attributed to the process of fibril dewatering; the resulting anisotropy of the membrane will also favor the swelling in one direction.[33] The clearer exposure of this lamellar structure for SDAC1 and SDAC2 indicate lower out-of-plane strength for these membranes with a lower charge. The lamellar structure is probably created during the preparation of the cross-sections and is not necessarily there without the mechanical action. This is also supported by the nanoporous structure as shown earlier.

3.5. Ionic Transport Properties

The ionic conductivity was found to increase with increasing sulfonate group content in the membranes (**Figure 8**a). This may be due in part to the increased charge content in the membranes per se, and in part due to the increased swelling and water content forming channels readily available for ionic transport. There is a linear relationship between the ionic conductivity and the swelling of the membrane (Figure 8b) indicating that water uptake has a major role for the membrane conductivity. Normalizing the ionic conductivity with the water uptake of the membranes reveals similar values of 4–6 mS cm^{-1} for all sulfonation levels (Figure S10, Supporting Information).

The membrane potential and corresponding cation transport number were found to increase slightly with higher sulfonate group content. The improved Donnan coion exclusion resulting from a higher fixed charge density in the membranes pores can be counteracted somewhat by increased water uptake and swelling. To be able to improve the selectivity

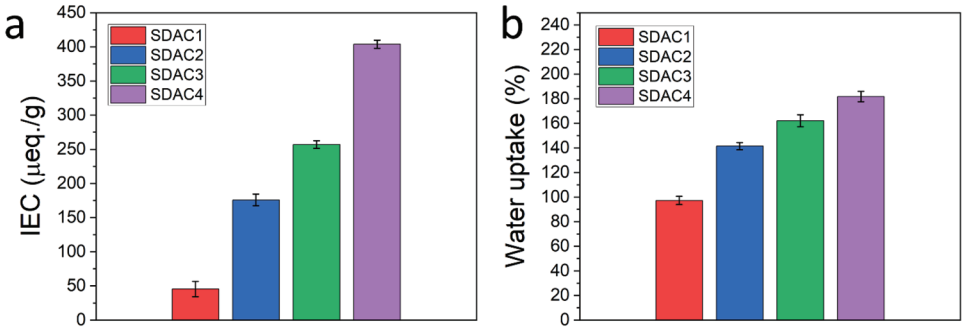

Figure 4. a) Ion exchange capacity and b) water uptake of sulfonated cellulose membranes SDAC1–4.

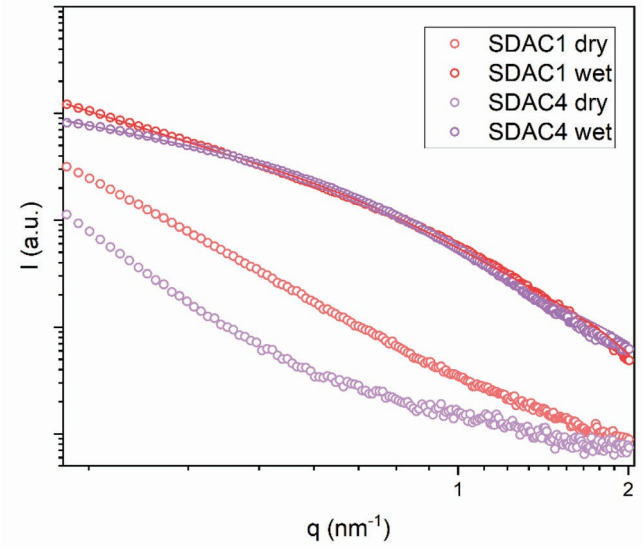

Figure 5. Radial integration of 2D SAXS patterns for SDAC1 and SDAC4 in dry and wet state respectively. Solid lines are fits to the data using Equation (1).

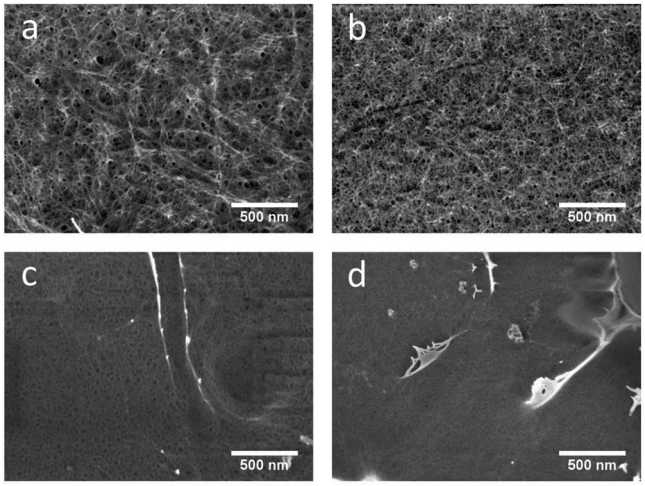

Figure 6. SEM-images showing the nanoporous surface structure of the sulfonated CNF membranes: a) SDAC1, b) SDAC2, c) SDAC3, and d) SDAC4.

further by increasing sulfonate group content, a higher degree of crosslinking may be needed to prevent excessive swelling. Membranes produced from CNFs with a higher selectivity than reported here have been demonstrated by using additives that introduce both charged groups and crosslinking functionality.[11]

The nanodimension of the pores (≈3 nm) in our sulfonated cellulose membranes suggests that the condition for ion transport might be close to the one observed in single charged nanopores[31] in which the interfacial ionic transport at the electrolyte-charged solid interface can play a major role when the ion concentration in the liquid electrolyte is low. Indeed, the requirement of charge neutrality within the channel will cause the concentration of mobile counterions in the channel to exceed that in the external bulk electrolyte. As a result, when the conductivity of the nanopores is measured versus the external bulk concentration of the electrolyte, the conductivity first decreases for lower concentration because the bulk transport of the nanopores dominate, but for a certain concentration of electrolyte, the bulk conductivity in the pores is smaller than the surface conductivity at the charged nanopores/electrolyte interface, such that the conductivity saturates at low concentration.[21]

The sulfonated cellulose membrane resistance is measured using electrochemical impedance spectroscopy and the concentration of the KCl electrolyte is varied. Figure 8c displays a conductivity saturation for low concentration of electrolyte that suggests the presence of this peculiar nanochannel conduction phenomenon.[34,35] Although this has been predicted theoretically,[36] this is the first time it is observed for ion transport across a synthetic cellulose membrane. Note however, that a similar phenomenon has been recently demonstrated in delignified wood forming nanofluidic membrane that inherits the nanofiber alignment direction from natural wood.[37]

The surface charge of the nanochannel walls was estimated via the ion exchange capacity and the fibril dimensions assuming that the CNF cross-sections are square with sides of equal length.[38] The surface area of a fibril can thus be calculated and combined with the cellulose density and ion exchange capacity to obtain an estimate of the amount of surface charge for a fibril, corresponding to the surface charge of the pore walls in the membrane. Here the surface charges are estimated

Table 4. Comparison of pore sizes obtained from liquid–liquid porometry and fitting of SAXS data.

Membrane	Mean flow pore size (porometry) [nm]	Pore size (SAXS, water swollen) [nm]
SDAC1	2.5	3.0
SDAC2	2.6	–
SDAC3	2.4	–
SDAC4	2.5	3.2

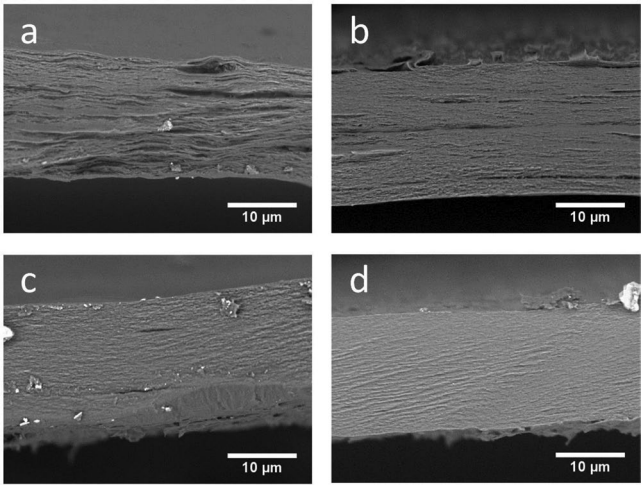

Figure 7. SEM-images showing cross-sections of sulfonated CNF membranes a) SDAC1, b) SDAC2, c) SDAC3, and d) SDAC4.

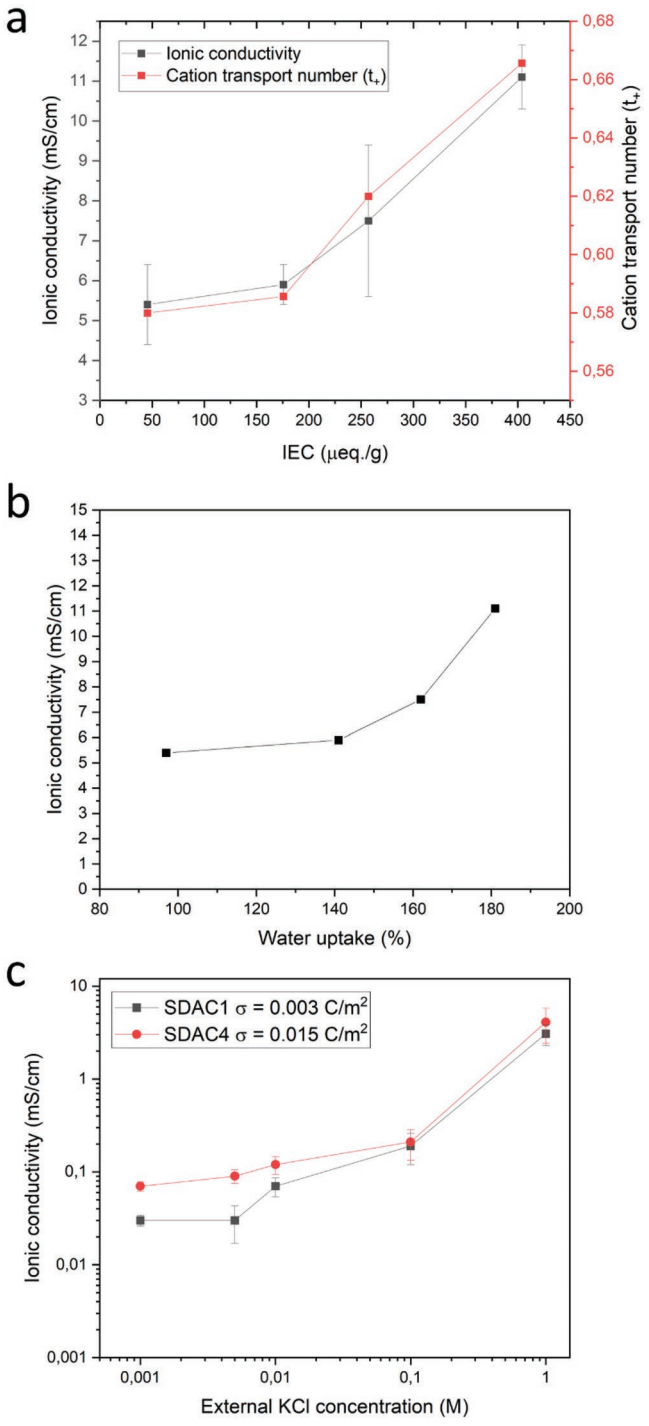

Figure 8. a) Ionic conductivity of membranes calculated from membrane resistance measured by linear sweep voltammetry in 0.5 M KCl (Figure S12, Supporting Information), and cation transport numbers, plotted as a function of the ion exchange capacity of the membranes. b) Ionic conductivity as a function of the membrane water uptake. Ionic conductivity of membranes calculated from membrane resistance measured by electrochemical impedance spectroscopy (Figure S13, Supporting Information) as a function of external electrolyte (KCl) concentration for SDAC1 and SDAC4 membranes. The estimated surface charge of the membrane pores is denoted σ.

to be $\sigma = 0.003$ C m^{-2} for SDAC1 and 0.015 C m^{-2} for SDAC4. The surface charge is expected to affect the value at which the conductivity saturates, as it controls the amount of counterions present in the nanochannels, which dominate the ionic conductivity at low external concentrations. This has been predicted theoretically[36] and this is observed experimentally here, the ionic conductivity of SDAC4 saturates at a higher value (0.07 mS cm^{-1}) than that of SDAC1 (0.03 mS cm^{-1}). This observation further supports the importance of the surface conduction in the charged sulfonated nanopores of the membrane.

3.5.1. Relation Structure-Porosity-Ion Transport

The pore sizes obtained by porometry and SAXS for the CNF membranes in dry and wet state along with the observation of ionic conductivity saturation at low electrolyte concentrations characteristic for ionic transport in nanochannels indicate that in this type of membrane it is indeed the interspace between the nanofibrils that determines the dominating scale of the porosity. Precise control of the pore size through packing, charge repulsion, and cross-linking is thus important for the possibility to design cellulose-based membranes with selective transport of certain species based at least partially on size-exclusion of large solutes. This is for instance the case in applications such as organic redox flow batteries, where the organic dyes should not cross-over the membrane.[39] The observation that the nanoscale of the pores is maintained in the water swollen state is equally of importance in systems requiring selective membranes while employing aqueous electrolytes. We have in our previous work shown that this type of CNF membranes may be promising for use in aqueous organic redox flow batteries[19] owing to their combination of wet stability, small pores, and favorable ionic transport properties. In the work presented herein we are able to explain more extensively the relation between the membrane properties and the ionic transport in the nanochannels. To fully understand the transport mechanisms governing crossover in more complicated systems such as redox flow batteries and how they relate to properties of the membrane is an exciting direction of research for this new research track.

4. Conclusions

In this work we show that oxidatively sulfonated cellulose nanofibrils of 3 nm in diameter and several hundred nm long can form a stable and very compact membrane where the porosity is governed by the distance between the stack nanofibers and the interstitial nm-scale voids between the nanofibrils. The largest pores are about 3 nm in size (by porometry and SAXS) and thus of the same dimension as sulfonated voids in Nafion. The fact that the nanofibrils are chemically cross-linked makes the membrane stable in water due to limited swelling. These properties explain the ability of those membranes to function in organic redox flow battery by both preventing the cross-over of large organic dyes and enabling good transport for small atomic cations as demonstrated in our previous work.

The membrane water content is found to increase with the sulfonation degree, which is expected since sulfonated groups are highly hydrophilic. Because water induced swelling in the nanofibril network, there is a correlation between the sulfonation degree and the pore size as indicated by SAXS. The measured ionic conductivity as a function of external electrolyte concentration shows conductivity saturation at low external electrolyte concentration, which reveals a significant contribution of the surface conductivity taking place at the interface between the charged cellulose pore surface and the liquid electrolyte inside the pores.

At high electrolyte concentration, the dominant transport is the volume conductivity in the liquid phase of the filled pores. Hence, the ratio between the two contributions to the ionic transport, one surface conductivity and one volume conductivity, depends on the sulfonation degree and the electrolyte concentration. When the sulfonation degree increases the pores acquire a high density of negative charges which should enhance the surface conductivity, but the membrane absorbs more water at the same time. The resulting swelling is translated into pore size an increase and volume conductivity enhancement. This opposite interplay between charge density and water uptake leads to a small effect on ionic selectivity and transport number; but an overall rise in ionic conductivity. To be able to improve the selectivity further, by increasing sulfonate group content, a higher degree of crosslinking may be needed to prevent excessive swelling.

To conclude, by varying the sulfonation degree, one can control and tune both physicochemical and ionic transport properties of sulfonated cellulose membranes, which show the possibility to use this material with high precision in rationally designed membranes for different end-use purposes.

Supporting Information

Supporting Information is available from the Wiley Online Library or from the author.

Acknowledgements

The authors want to thank VINNOVA (Digital Cellulose Center), BillerudKorsnäs, the Knut and Alice Wallenberg foundation (KAW 2019.0604 and KAW 2021.0195), Vetenskaprådet (2016-05990), the Wallenberg Wood Science Center, and the Swedish Government Strategic Research Area in Materials Science on Advanced Functional Materials at Linköping University (Faculty Grant SFO-Mat-LiU No. 2009-00971) for financial funding. The authors also thank POROMETER Application Laboratory for the measurement of porosity and Benselfelt SciArt for the illustration of the membrane.

Conflict of Interest

The authors declare no conflict of interest.

Data Availability Statement

The data that support the findings of this study are available from the corresponding author upon reasonable request.

Keywords

crosslinked sulfonated nanocelluloses, ionic transport, pore sizes, selective membranes, water uptake

Received: June 17, 2022
Revised: July 26, 2022
Published online:

[1] H. Prifti, A. Parasuraman, S. Winardi, T. M. Lim, M. Skyllas-Kazacos, *Membranes* **2012**, *2*, 275.
[2] S. P. Nunes, P. Z. Culfaz-Emecen, G. Z. Ramon, T. Visser, G. H. Koops, W. Jin, M. Ulbricht, *J. Membr. Sci.* **2020**, *598*, 117761.
[3] J. Noack, L. Wietschel, N. Roznyatovskaya, K. Pinkwart, J. Tübke, *Energies* **2016**, *9*, 627.
[4] S. A. Muhmed, N. A. M. Nor, J. Jaafar, A. F. Ismail, M. H. D. Othman, M. A. Rahman, F. Aziz, N. Yusof, *Energ. Ecol. Environ.* **2020**, *5*, 85.
[5] S. Adhikari, M. K. Pagels, J. Y. Jeon, C. Bae, *Polymer* **2020**, *211*, 123080.
[6] R. S. L. Yee, R. A. Rozendal, K. Zhang, B. P. Ladewig, *Chem. Eng. Res. Des.* **2012**, *90*, 950.
[7] E. J. Foster, R. J. Moon, U. P. Agarwal, M. J. Bortner, J. Bras, S. Camarero-Espinosa, K. J. Chan, M. J. D. Clift, E. D. Cranston, S. J. Eichhorn, D. M. Fox, W. Y. Hamad, L. Heux, B. Jean, M. Korey, W. Nieh, K. J. Ong, M. S. Reid, S. Renneckar, R. Roberts, J. A. Shatkin, J. Simonsen, K. Stinson-Bagby, N. Wanasekara, J. Youngblood, *Chem. Soc. Rev.* **2018**, *47*, 2609.
[8] S. S. Ahankari, A. R. Subhedar, S. S. Bhadauria, A. Dufresne, *Carbohydr. Polym.* **2021**, *255*, 117479.
[9] Z. Karim, S. Claudpierre, M. Grahn, K. Oksman, A. P. Mathew, *J. Membr. Sci.* **2016**, *514*, 418.
[10] A. Mautner, K.-Y. Lee, T. Tammelin, A. P. Mathew, A. J. Nedoma, K. Li, A. Bismarck, *React. Funct. Polym.* **2015**, *86*, 209.
[11] H. Yang, J. Edberg, V. Gueskine, M. Vagin, M. G. Say, J. Erlandsson, L. Wågberg, I. Engquist, M. Berggren, *Carbohydr. Polym.* **2022**, *278*, 118938.
[12] J. Erlandsson, T. Pettersson, T. Ingverud, H. Granberg, P. A. Larsson, M. Malkoch, L. Wågberg, *J. Mater. Chem. A* **2018**, *6*, 19371.
[13] P. A. Larsson, T. Pettersson, L. Wågberg, *Green Mater.* **2014**, *2*, 163.
[14] T. Bayer, B. V. Cunning, R. Selyanchyn, M. Nishihara, S. Fujikawa, K. Sasaki, S. M. Lyth, *Chem. Mater.* **2016**, *28*, 4805.
[15] V. Guccini, A. Carlson, S. Yu, G. Lindbergh, R. W. Lindström, G. Salazar-Alvarez, *J. Mater. Chem. A* **2019**, *7*, 25032.
[16] A. Mukhopadhyay, Z. Cheng, A. Natan, Y. Ma, Y. Yang, D. Cao, W. Wang, H. Zhu, *Nano Lett.* **2019**, *19*, 8979.
[17] T. Nypelö, B. Berke, S. Spirk, J. A. Sirviö, *Carbohydr. Polym.* **2021**, *252*, 117105.
[18] T. Bayer, B. V. Cunning, B. Šmíd, R. Selyanchyn, S. Fujikawa, K. Sasaki, S. M. Lyth, *Cellulose* **2021**, *28*, 1355.
[19] S. Lander, M. Vagin, V. Gueskine, J. Erlandsson, Y. Boissard, L. Korhonen, M. Berggren, L. Wågberg, X. Crispin, *Adv. Energy Sustainability Res.* **2022**, 2200016.
[20] N. P. Berezina, N. A. Kononenko, O. A. Dyomina, N. P. Gnusin, *Adv. Colloid Interface Sci.* **2008**, *139*, 3.
[21] J. Kamcev, D. R. Paul, G. S. Manning, B. D. Freeman, *Macromolecules* **2018**, *51*, 5519.
[22] V. López Durán, J. Erlandsson, L. Wågberg, P. A. Larsson, *ACS Sustainable Chem. Eng.* **2018**, *6*, 9951.
[23] M. C. R. Symons, *J. Chem. Soc.* **1955**, 2794.
[24] P. A. Larsson, M. Gimåker, L. Wågberg, *Cellulose* **2008**, *15*, 837.
[25] D. Zhang, C. Courchene, X. Chai, A. J. Ragauskas, TAPPI Engineering, Pulping Environmental Conf. Proc., Tappi Press, Atlanta **2006**.
[26] H. Liimatainen, J. Sirviö, O. Sundman, O. Hormi, J. Niinimäki, *Water Res.* **2012**, *46*, 2159.
[27] *Introduction to Organic Spectroscopy*, (Ed: J. B. Lambert), Macmillan Publ. Company, New York, NY **1987**.

[28] T. Saito, S. Kimura, Y. Nishiyama, A. Isogai, *Biomacromolecules* **2007**, *8*, 2485.
[29] L. Wågberg, G. Decher, M. Norgren, T. Lindström, M. Ankerfors, K. Axnäs, *Langmuir* **2008**, *24*, 784.
[30] J. Zhang, N. Jiang, Z. Dang, T. J. Elder, A. J. Ragauskas, *Cellulose* **2008**, *15*, 489.
[31] R.-M. P. Karlsson, P. T. Larsson, P. Hansson, L. Wågberg, *Biomacromolecules* **2019**, *20*, 1603.
[32] L. Valencia, S. Monti, S. Kumar, C. Zhu, P. Liu, S. Yu, A. P. Mathew, *Nanoscale* **2019**, *11*, 22413.
[33] T. Benselfelt, L. Wågberg, *Biomacromolecules* **2019**, *20*, 2406.
[34] D. Stein, M. Kruithof, C. Dekker, *Phys. Rev. Lett.* **2004**, *93*, 035901.
[35] K. Xiao, L. Jiang, M. Antonietti, *Joule* **2019**, *3*, 2364.
[36] M. Garg, I. Zozoulenko, *ACS Appl. Bio Mater.* **2021**, *4*, 8301.
[37] T. Li, S. X. Li, W. Kong, C. Chen, E. Hitz, C. Jia, J. Dai, X. Zhang, R. Briber, Z. Siwy, M. Reed, L. Hu, *Sci. Adv.* **2019**, *5*, 4238.
[38] Y. Okita, T. Saito, A. Isogai, *Biomacromolecules* **2010**, *11*, 1696.
[39] L. Hu, L. Gao, M. Di, X. Jiang, X. Wu, X. Yan, X. Li, G. He, *Energy Storage Mater.* **2021**, *34*, 648.